Powder Technology 233 (2013) 72–79

Contents lists available at SciVerse ScienceDirect

Powder Technology

journal homepage: www.elsevier.com/locate/powtec

Development and application of oxide-based flux powder for tungsten inert gas welding of austenitic stainless steels

Kuang-Hung Tseng *

Institute of Materials Engineering, National Pingtung University of Science and Technology, Pingtung 91201, Taiwan

ARTICLE INFO

Article history:
Received 7 July 2012
Received in revised form 28 August 2012
Accepted 31 August 2012
Available online 7 September 2012

Keywords:
Oxide-based flux powder
Alcohol solvent
Coating density
Arc pressure
Finger-like penetration profile

ABSTRACT

The experiments reported in this study involved using a new activated flux developed by the National Pingtung University of Science and Technology (NPUST) to systematically investigate the influence of oxide-based flux powder and carrier solvent composition on the surface appearance, geometric shape, angular distortion, and ferrite content of austenitic 316L stainless steel tungsten inert gas (TIG) welds. The flux powders comprising oxide, fluoride, and sulfide mixed with methanol or ethanol achieved good spreadability. For the investigated currents of 125 to 225 A, the maximum penetration of stainless steel activated TIG weld was obtained when the coating density was between 0.92 and 1.86 mg/cm^2. The depth of finger-like profile in the conventional TIG weld increased in conjunction with the current because of the induced strong arc pressure. The arc pressure also raised the penetration capability of activated TIG welds at high currents. The results show that higher current levels have lower ferrite content of austenitic 316L stainless steel weld metal than lower current levels.

© 2012 Elsevier B.V. All rights reserved.

1. Introduction

TIG welding is considered a reliable process for welding numerous metals and alloys to ensure superior and almost defect-free weld quality because the electrode, arc, and molten metal are shielded by an inert envelope of argon or helium gas. It has become a popular choice for arc welding processes when high-quality welds are required. TIG welding applications include welding of sheet, plate, tube, and castings for use in nuclear, aerospace, power generation, shipbuilding, and other industries. TIG welding can be operated using filler metals to produce thick section welds. Autogenous welds (welds without the addition of any filler metals) can be applied for thin sections. The primary limitation of TIG welding is low productivity because of its low deposition rate and shallow joint penetration. The inability for TIG welding to produce deep penetration welds limits the thickness of workpieces that can be reliably joined to less than approximately 3 mm [1,2]. Workpieces greater than 3 mm typically require joint edge preparation and multiple passes to completely fill the joint. TIG welds are also affected by heat-to-heat compositional variation in the base metal being welded.

The depth and consistency of penetration in TIG welds can be improved by applying a thin layer of activated flux in the form of thin paste to the workpiece surface prior to welding [3–5]. The heat of the TIG arc melts and vaporizes part of the flux as arc passes over the flux. Consequently, the penetration depth can be increased up to three times for a given level of heat input. The earliest reference to activated flux assisted TIG (activated TIG) welding was published in 1965 and discussed using an activated flux to improve the penetration depth of titanium alloy welds [6]. This flux comprised fluorides and chlorides of alkali and alkali-earth metals. Activated fluxes have recently become commercially available for industrial applications. Commercially available fluxes are claimed to be suitable for the welding of various materials, including C–Mn steels, Cr–Mo steels, Ni–Cr–Mo steels, stainless steels, nickel-based alloys, and titanium alloys.

An activated flux is a mixture of flux powder suspended in carrier solvent. The composition of flux powder has a critical function in increasing the penetration depth of activated TIG welds. Although several mechanisms have been postulated that explain why an activated flux achieves increased weld penetration [7], extant literature on flux formulations for activated TIG welding is rare, possibly because of commercial reasons. Moreover, the few formulations that have been identified are complex [8]. In addition to TIG welding parameters being the primary factors in determining the level of quality and productivity, they affect the penetration improvement function of the activated flux. High-quality welds can be achieved by meeting quality requirements such as weld geometry, which is highly influenced by various TIG welding process parameters [9]. Inadequate weld geometry may contribute to the failure of a welded structure [10].

Despite the productivity benefits of activated TIG welding, the industry has been slow to exploit this process, partially because activated TIG welding tends to produce an inferior surface finish compared to conventional TIG welding. Moreover, knowledge on the relationship between process parameters and weld quality is essential for

* No. 1, Hseuhfu Rd., Neipu, Pingtung 91201, Taiwan. Tel.: +886 8 7703202; fax: +886 8 7740552.
E-mail address: tkh@mail.npust.edu.tw.

0032-5910/$ – see front matter © 2012 Elsevier B.V. All rights reserved.
http://dx.doi.org/10.1016/j.powtec.2012.08.038

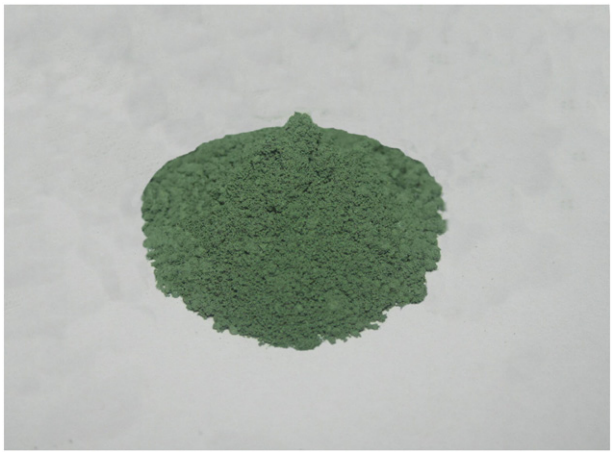

Fig 1. Original appearance of oxide-based flux powder.

Table 1
Composition of oxide-based flux.

SiO_2	TiO_2	Cr_2O_3	MoO_3	NiF_2	MoS_2
30 wt.%	25 wt.%	25 wt.%	10 wt.%	5 wt.%	5 wt.%

Table 2
Process parameters of TIG welding experiment.

Weld current	125 A, 150 A, 175 A, 200 A, 225 A
Travel speed	175 mm/min
Electrode gap	3 mm
Shielding gas	Argon
Gas flow rate	12 l/min

controlling the quality and performance in the activated TIG welds. The experiments reported in this study used a novel activated flux developed by the NPUST to systematically investigate the influence of oxide-based flux powder and carrier solvent composition on the surface appearance, geometric shape, angular distortion, and ferrite content of austenitic 316L stainless steel TIG welds. This study also discusses the relationship between the process parameters and the quality performances of activated TIG welding.

2. Experimental details

Austenitic 316L stainless steel with the chemical composition (in wt.%) of 0.019% C, 0.49% Si, 1.76% Mn, 0.031% P, 0.002% S, 17.11% Cr, 10.10% Ni, 2.04% Mo, 0.042% N, and balance Fe was used as base metal. Plates 6 mm in thickness were cut into strips of size 100 × 100 mm, which were roughly grinded with 240 grit silicon carbide abrasive paper to remove all impurities, and were subsequently cleaned with acetone prior to welding.

A commercial flux powder comprising silicon dioxide (SiO_2), titanium dioxide (TiO_2), chromium oxide (Cr_2O_3), molybdenum trioxide (MoO_3), nickel fluoride (NiF_2), and molybdenum disulphide (MoS_2) has been developed by the NPUST, Taiwan [11]. Fig. 1 shows an original appearance of oxide-based flux powder. Table 1 lists the composition of the flux powder. Prior to welding, the flux powder was uniformly mixed with carrier solvent to form a paint-like consistency, and was subsequently manually applied with a paintbrush as a sufficient layer thick to prevent visual observation of the base metal beneath.

A direct-current, electrode-negative power supply device was used with a mechanized operation system in which the welding torch traveled at a constant speed. Single-pass, autogenous TIG welding was performed along the centerline of the test specimen to produce a bead-on-plate weld. A water-cooled torch with a standard 2% thoriated tungsten electrode rod with a 3.2 mm diameter was used. The electrode tip was a blunt point with a 45° angle. Argon of 99.99% purity was used as shielding gas. Table 2 lists the process parameters used in TIG welding experiments. The tip angle of electrode rod was grounded, and the electrode gap was measured for each new weld prior to welding to ensure that the welding experiment was performed under the same operating conditions. During welding, a digital data acquisition system with a sampling rate of 120 samples per second was used to continuously measure the weld current and the arc voltage.

All test specimens were constraint-free during welding to avoid the influence of reaction stresses. Following welding, experiments were conducted to measure the angular distortion in a bead-on-plate welded plate. The angular distortion of the weldment was measured using the mean vertical displacement, as Fig. 2 illustrates. A hole was drilled from the back at points P_1, P_2, and P_3, and a pillar was inserted into each hole. These three pillars (one stable, the other two adjustable) were used to adjust the horizontal level, and the distance from each point to the horizontal surface was then recorded. Measurements were taken before and after welding. The differences in measurements before and after welding revealed the

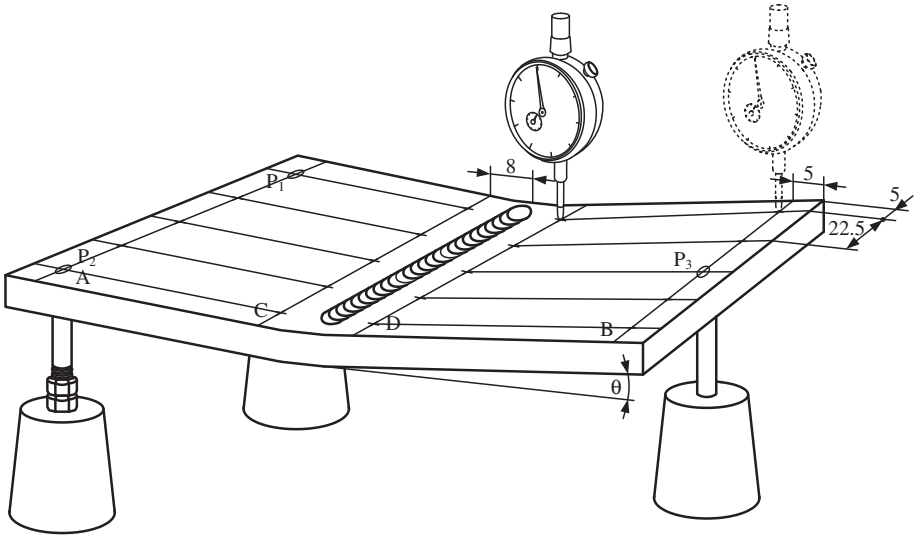

Fig. 2. Schematic diagram of distortion measurement.

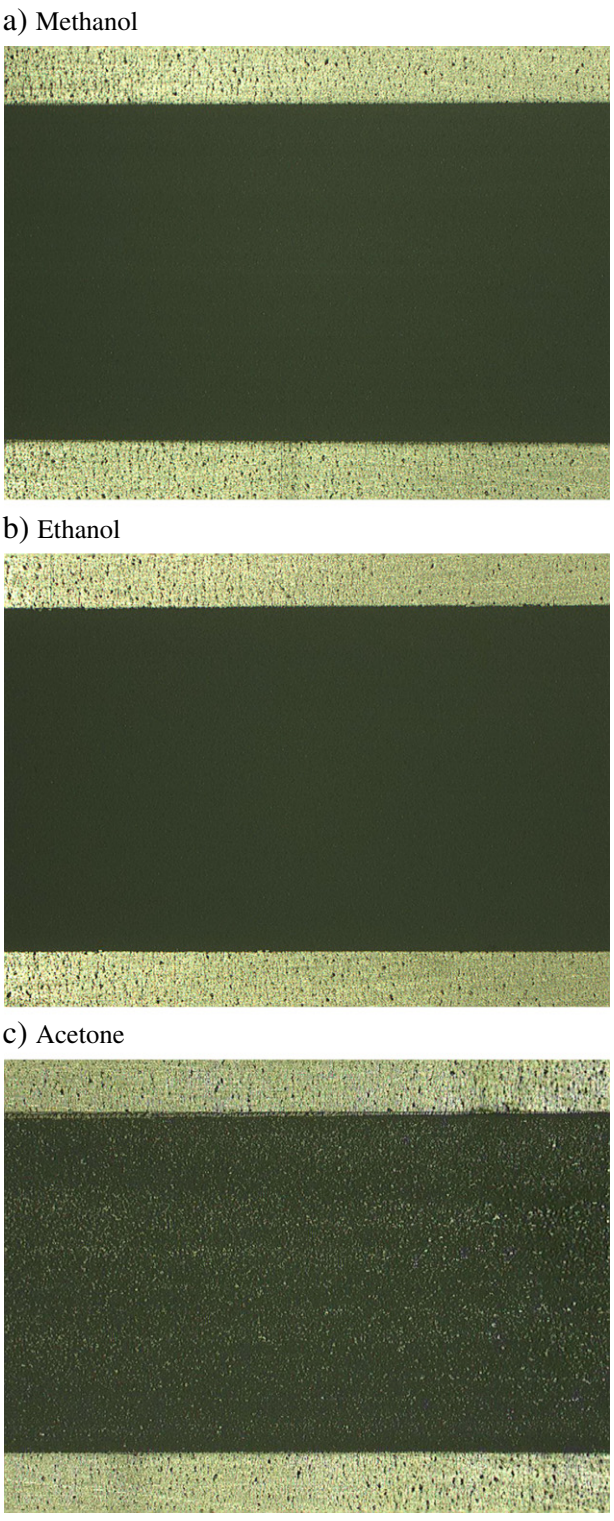

Fig. 3. Effect of carrier solvent on spreadability of activated flux.

vertical displacement caused by welding, and the angular distortion (θ) was derived using the following equation.

$$\theta = 2 \times \tan^{-1} \frac{|(A+B)-(C+D)|}{50} \quad (1)$$

where A, B, C, and D represent the mean vertical displacement values of each point.

Table 3
Characteristic of carrier solvent.

Carrier solvent	Methanol	Ethanol	Acetone
Viscosity (20 °C, mPa·s)	0.817	1.770	0.389
Vapor pressure (20 °C, mm Hg)	96	44	184

Ferrite number (FN) is an arbitrary standardized value designating the ferrite content in the austenitic stainless steel weld metal or base metal. In this study, FN was measured using a ferritoscope. This device detects phases such as ferrite according to the magnetic susceptibility, which differs from that of paramagnetic austenite. To minimize measurement errors resulting from inhomogeneity in the weld metals, the average value of seven measurements from various locations along the as-welded surface was calculated.

In this study, the surface appearance and geometric shape of the welds were photographed with a stereomicroscope. The transverse sections were made at various locations along the welds, whereas samples for metallographic examination were prepared using standard procedures, including sectioning, mounting, grinding, and polishing to a 0.3 μm finish, followed by electrolytic etching in an electrolyte solution consisting of 10 g oxalic acid and 100 ml water. Each sample was examined with a toolmaker's microscope to measure the penetration depth and bead width. Each data point represents the average of three samples.

3. Results and discussion

3.1. Evaluation on carrier solvent of activated flux

The oxide-based flux is provided as a fine powder that is mixed with a suitable solvent. In this experiment, methanol, ethanol, and acetone were used as a carrier solvent. Furthermore, the 1500 mg flux powder was uniformly mixed with 1.5 ml of carrier solvent to form a paste and applied to a stainless steel plate surface (the ratio of flux powder to carrier solvent is not critical, although it must be mixed to a consistency that can be "painted" on). The result in Fig. 3 clearly shows that the oxide-based flux powder mixed with methanol or ethanol provides good spreadability and coverability. Table 3 lists the characteristics of the experimental solvents. The viscosity of methanol or ethanol is substantially higher than that of acetone and promotes the cohesive force of the mixture. Consequently, the flux powder mixed with methanol or ethanol has a uniform coating distribution. Moreover, a substance with a high vapor pressure at normal

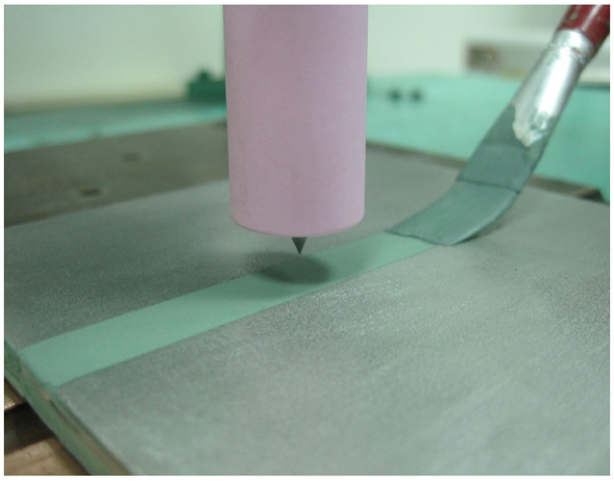

Fig. 4. Activated flux applied with a paintbrush.

temperatures is frequently described as volatile. The vapor pressure of methanol is higher than that of ethanol and promotes the drying time of the mixture. Based on the results, the oxide-based flux powder should be mixed with alcohol solvent (preferably methanol) to form a paste that is easy to apply with a paintbrush to the parts to be welded (Fig. 4).

Chern et al. reported that the use of the activated fluxes tends to create excessive residual slag and spatters on the surface of the activated TIG welds [4]. Fig. 5 shows that a smooth, clean surface appearance of stainless steel activated TIG welds can be achieved when using the flux powders comprising oxide, fluoride, and sulfide mixed with a methanol.

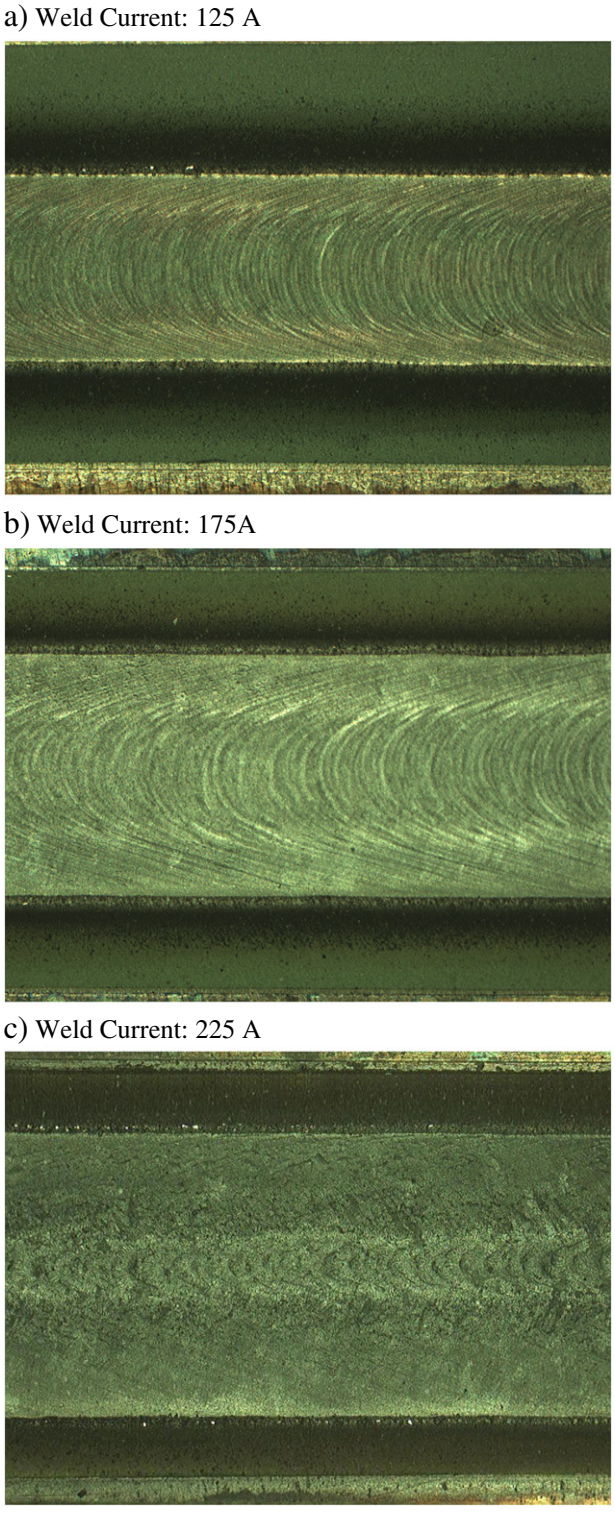

Fig. 5. Surface appearance of activated TIG welds at different current levels.

3.2. Evaluation on coating density of activated flux

The activated flux coating density has a highly significant effect on the penetration depth of the stainless steel activated TIG welds (Fig. 6). The penetration depth initially increases sharply with coating density before becoming approximately constant and subsequently decreases. The penetration depth of conventional TIG welds corresponds to zero coating density and ranges from 0.80 to 2.85 mm at the investigated currents (125 to 225 A). Depending on the weld current, the maximum penetration depth of stainless steel activated TIG weld is obtained when the coating density ranges from 0.92 to 1.86 mg/cm^2. The measured maximum penetration depths are 2.55 and 7.13 mm at 125 and 225 A, respectively. This result indicates that the optimal activated flux coating density increases with the current. Beyond the optimal coating density, the penetration depth remains approximately constant before decreasing. This reduction is attributable to the higher arc heat energy consumption required to melt the thick flux barrier.

3.3. Effect of process parameter on geometric shape of weld

Fig. 7 shows the effect of process parameters on the geometric shape of stainless steel TIG welds produced with and without an activated flux. A series of experiments were conducted at various weld currents from 125 to 225 A. All remaining process parameters were constant. In addition, the coating density of the activated flux was approximately 3.64 mg/cm^2. Significant variation in the penetration depth and bead width of the TIG weld occurred. As the current increased from 125 to 225 A, the penetration depth of the conventional TIG weld increased from 0.80 to 2.85 mm and the bead width increased from 6.47 to 11.02 mm. This result indicates that TIG welds produced without an activated flux result in a wide, shallow shape. However, as the current increased from 125 to 225 A, the penetration depth increased from 2.51 to 7.08 mm and the bead width increased from 4.88 to 6.92 mm. This result indicates that activated TIG welds exhibit a narrow, deep shape.

A fusion zone geometry schematic diagram was developed to clarify the relationship between weld geometry and the applied activated flux. Fig. 8 shows that the weld geometry in this study is characterized using

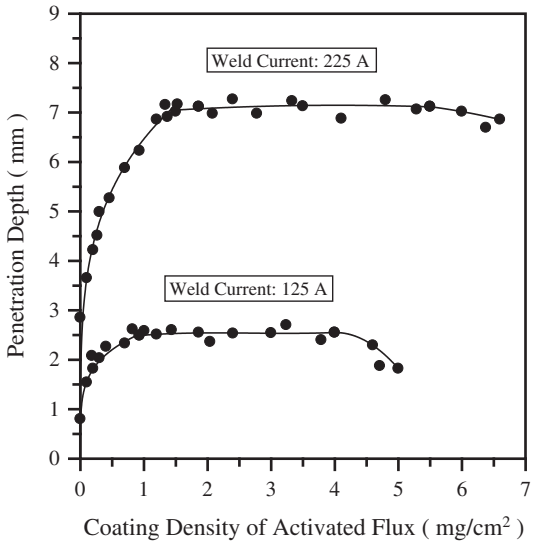

Fig. 6. Effect of coating density on penetration depth of TIG weld.

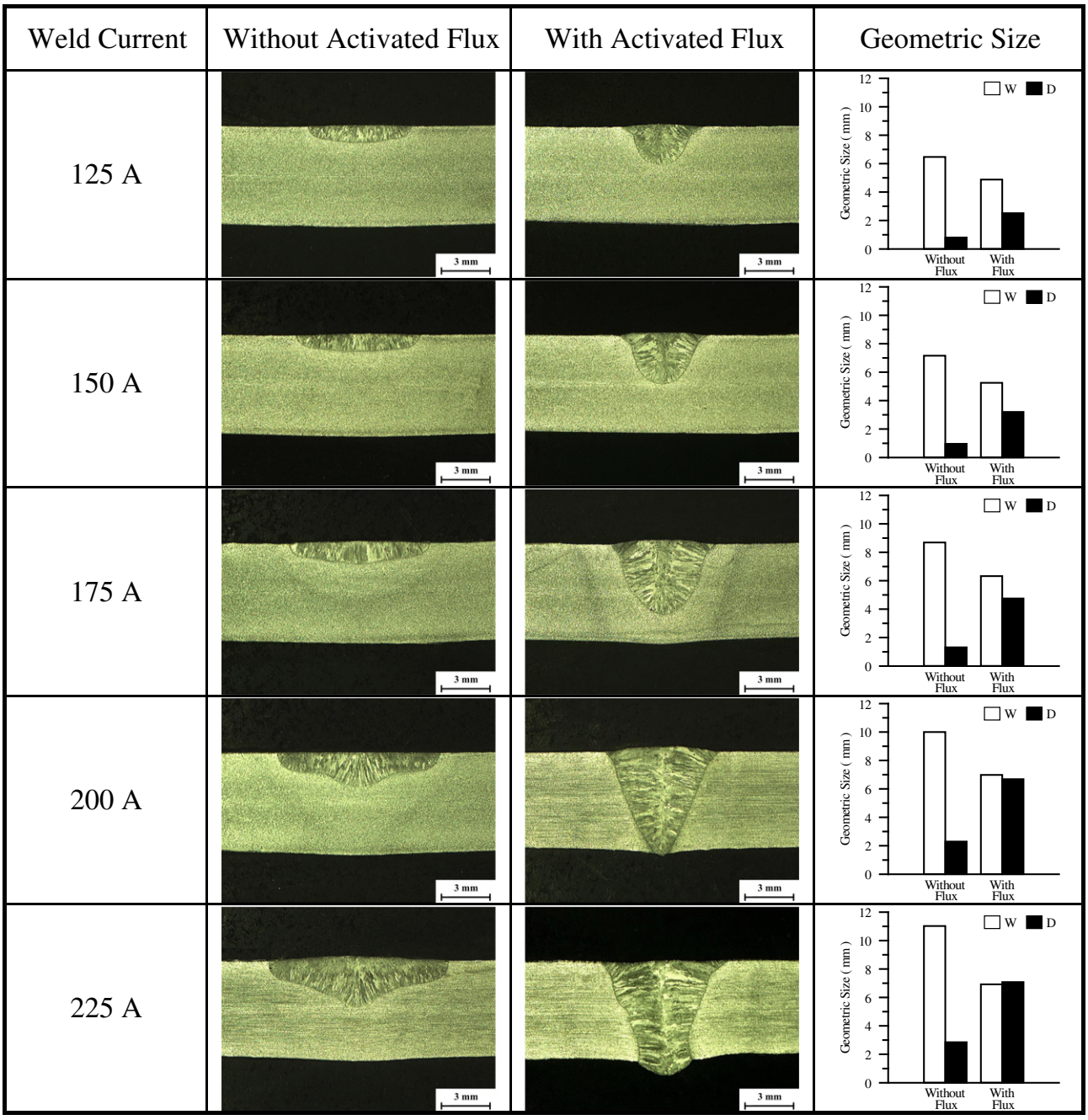

Fig. 7. Effect of weld current on geometric shape of TIG weld.

the following three parameters: penetration depth D, bead width W, and reinforcement R. Moreover, the weld depth-to-width ratio is defined as $K=(R+D)/W$. Kc is the D/W of conventional TIG welding,

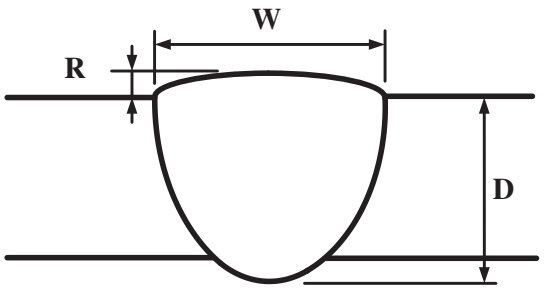

Fig. 8. Schematic representation of weld geometry.

and Ka is the D/W of activated TIG welding. Larger Ka/Kc values represent greater improvements in weld geometry function of the applied activated flux. Fig. 9 shows that the activated flux can significantly increase the D/W of stainless steel TIG welds, in which the degree of improvement depends on the weld current. When the current is 125 A, $Ka=0.51$, and $Kc=0.12$, the weld depth-to-width ratio increases to a maximum of 425% of that for conventional TIG welding. When the current is 175 A, $Ka=0.75$, and $Kc=0.15$, the weld depth-to-width ratio increases to a maximum of 500% of that for conventional TIG welding. When the current is 225 A, $Ka=1.02$, and $Kc=0.26$, the weld depth-to-width ratio increases to a maximum of 392% of that for conventional TIG welding. These results show that the penetration improvement of the activated flux initially increases with the weld current before decreasing, implying that there is a critical point at which an optimal penetration improvement is achieved. In this experiment, when the current is 175 A, the penetration improvement of the

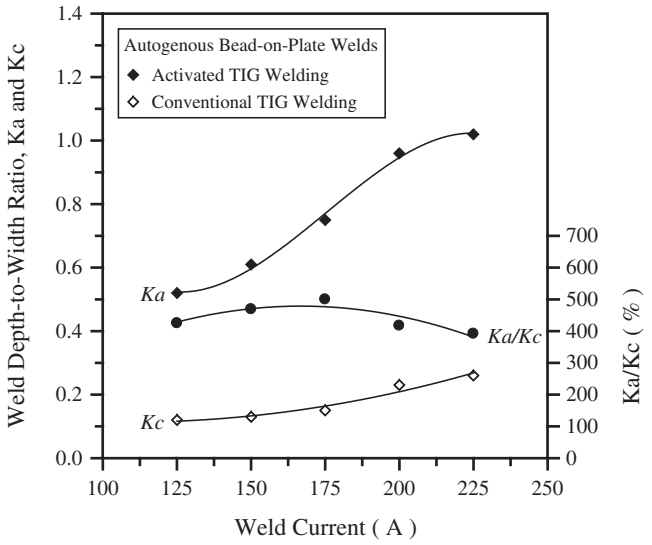

Fig. 9. Effect of weld current on depth-to-width ratio of TIG weld.

activated flux can be increased to a maximum of 500%. However, when the current is greater than 200 A, the penetration improvement of the activated flux decreases. This decrease is attributable to the higher currents forming a deep finger-like profile in conventional TIG welds, resulting in deeper penetration. This study proposes that the activated flux penetration improvement at higher currents is critical for activated TIG welding.

Although there is no consensus on the mechanism for increased penetration depth of the activated TIG weld, activated TIG welding is known to show a constriction of the arc column compared with the more diffuse conventional TIG welding at identical current levels. In addition, the oxygen from the decomposition of the oxide-based flux powder in the molten pool is known to induce the centripetal Marangoni convection by inverting the surface tension gradient of the molten pool. Tseng et al. made and compared experimental observations of interactive phenomena between the weld arc and the molten pool in activated and conventional TIG welding processes [1,2,4,5]. Fig. 10 illustrates a summary of the mechanism underlying the increased penetration capability of TIG weld produced with an activated flux.

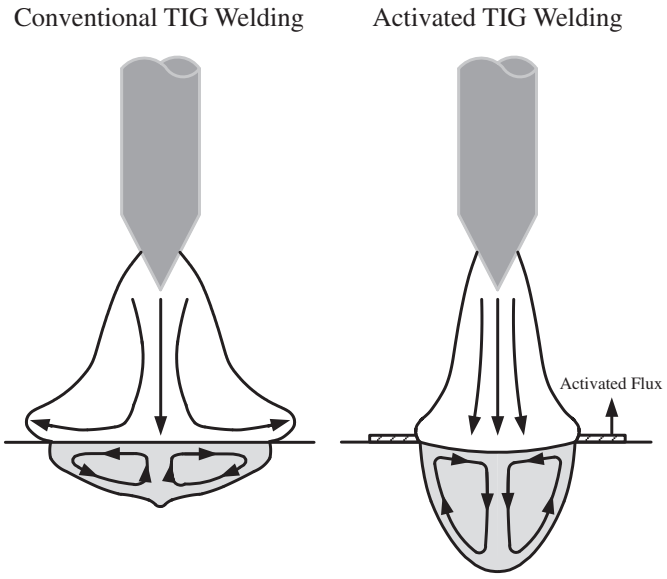

Fig. 10. Mechanism for increased penetration capability of activated TIG weld.

For higher current activated TIG welding processes, the constricted arc column raises the energy density of the heat source and generates a high current density at the molten pool surface. The resulting large electromagnetic force and high arc pressure contribute a forceful downward flow of heat within the molten pool (the arc pressure is generated when the plasma jet is arrested on the molten pool surface). Furthermore, the inward radial flow of the centripetal Marangoni convection further promotes the transfer of arc heat from the surface to the bottom of the molten pool and results in a higher weld depth-to-width ratio. However, the lower current activated TIG welding process cannot increase the current density significantly in the arc column. Thus, the electromagnetic force and arc pressure become very small, which has not led to a significant increase in the penetration capability of activated TIG welds. Although further investigation is required to understand the mechanisms, this study potentially shows the effect of current levels on the penetration capability of activated TIG weld.

3.4. Effect of arc pressure on weld geometry

Arc pressure also has a critical function in affecting the geometric shape of TIG welds [12]. Fig. 7 shows that a finger-like profile occurs in conventional TIG welds at currents greater than 200 A. This result is attributable to the arc pressure action. Arc pressure in TIG welding is caused by the momentum transfer of the impinging plasma jet on the molten pool surface and has been considered by numerous studies to be a major factor in producing surface depression, humping, and undercutting [13]. Arc pressure distribution on the molten pool surface in TIG welding processes has been investigated [14], and characterized as a Gaussian function (Fig. 11). This indicates that the maximum arc pressure is at the center of the molten pool surface. The electromagnetically induced arc pressure increases with the weld current. Consequently, the depth of the finger-like penetration increases with the weld current because of the induced strong arc pressure acting on the center of the molten pool surface. This result indicates that the finger-like profile of TIG weld is dominated by the

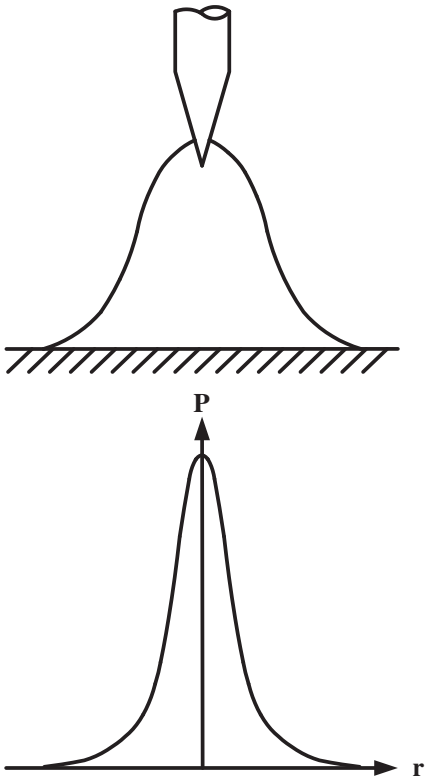

Fig. 11. Schematic representation of arc pressure distribution.

arc pressure. Moreover, the arc pressure induced by the plasma jet arrested on the center of the molten pool surface also enhances the centripetal Marangoni convection and increases the penetration capability of activated TIG welds. For a travel speed of 175 mm/min, full penetration of stainless steel TIG weld produced with oxide-based activated flux is achieved using currents greater than 200 A.

3.5. Effect of process parameter on angular distortion of weldment

Fig. 12 shows the effect of process parameters on the angular distortion of stainless steel TIG weldments produced with and without an activated flux. The results show that activated TIG welding is capable of reducing the angular distortion of stainless steel weldments. For conventional TIG welding, the angular distortion of stainless steel weldment increases with the weld current. This indicates that increasing the weld current to improve the penetration capability of the conventional TIG weld causes the weld shape to become excessively wide with a relatively minor increase in depth, resulting in a greater angular distortion of the weldment. For activated TIG weldments produced at a 125 A current, its penetration depth is less than half of the plate thickness. The shallow depth causes lower angular distortion of the weldment, and with increasing penetration depth to plate thickness ratio, the angular distortion of the activated TIG weldment at 150 A increases to a critical point (penetration depth to plate thickness ratio equivalent to 0.5), and when the penetration depth exceeds half of the plate thickness, the angular distortion of the activated TIG weldment decreases at currents greater than 175 A. Activated TIG welding increases the penetration depth and weld depth-to-width ratio, which indicates the arc with a higher energy density [5]. As the arc energy density increases, the overall heat required per unit length of weld deposit decreases. This contributes to a reduction in the quantity of supplied heat, thereby preventing the base material from overheating and reducing the incidence of thermal stress and incompatible strain caused by shrinkage in thickness. Consequently, activated TIG welding is capable of significantly reducing the angular distortion of weldments.

3.6. Effect of process parameter on ferrite content of weld

Fig. 13 shows the effect of process parameters on the ferrite content of stainless steel TIG weld metal produced with and without an activated flux. The weld metal of austenitic 316L stainless steel contains higher ferrite content than the base metal. This is because most of the weld metal of austenitic stainless steels solidifies as the delta-ferrite phase. During welding, the cooling rate of the weld metal is so rapid that the phase transformation of delta-ferrite phase to austenite phase is incomplete. Consequently, more delta-ferrite is retained in the weld metal after solidification. In addition, the ferrite content of stainless steel TIG welds produced with and without an activated flux decreases when the weld current increases. This is related to the magnitude of the heat input because a higher heat input can increase the peak temperature of weld metal and reduce its cooling rate. In other words, the most significant characteristic of heat input is how it influences the cooling rate in the weld metal, thereby affecting the solidification structures of the weld metal. The heat input per unit length of a weld increases with the weld current. High heat input results in a slow cooling rate and further promotes the transformation from the delta-ferrite phase to the austenite phase in the stainless steel weld metal. Consequently, higher current levels have lower ferrite content than lower current levels. Under the same TIG welding process parameters, furthermore, activated TIG welds have a higher ferrite content than conventional TIG welds. Activated TIG welding has a higher arc energy density, which is characterized by a lower heat input and a consequently rapid cooling rate. Thus, stainless steel activated TIG welds retain higher ferrite contents.

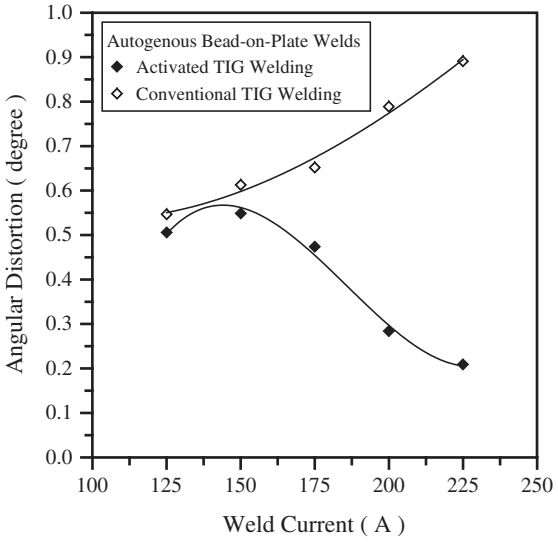

Fig. 12. Effect of weld current on angular distortion of TIG weldment.

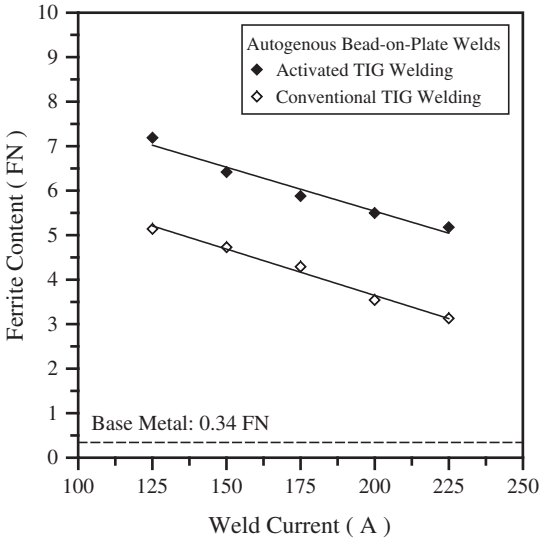

Fig. 13. Effect of weld current on ferrite content of TIG weld metal.

4. Conclusions

In this study, a novel activated flux that is easy to apply and provides good spreadability was developed; furthermore, it provides increased penetration capability and reduced angular distortion substantially independent of heat-to-heat compositional variations in austenitic 316L stainless steels. The results are summarized as follows:

1. In this study, the flux powders comprising oxide, fluoride, and sulfide mixed with methanol or ethanol provides good spreadability and coverability. A satisfactory surface appearance of the stainless steel activated TIG weld was obtained with the use of the discussed novel activated flux developed by the NPUST.
2. For the investigated currents of 125 to 225 A, the maximum penetration of stainless steel activated TIG weld is obtained for the coating density ranging between 0.92 and 1.86 mg/cm^2. The optimal coating density of activated flux increases with the weld current.

3. For conventional TIG welds, the depth of finger-like penetration increases with the weld current because of the induced strong arc pressure. The arc pressure also raises the penetration capability of activated TIG welds.
4. Full penetration and the maximal weld depth-to-width ratio result in the lowest angular distortion of the activated TIG weldment. This is because the arc heated the weld metal more evenly throughout the thickness of the weldment.
5. When the weld current increases, the ferrite content of stainless steel TIG welds produced with and without an activated flux decreases. High heat input results in a slow cooling rate and further promotes the transformation from the delta-ferrite phase to the austenite phase in stainless steel weld metal.

Acknowledgments

The authors gratefully acknowledge the financial support provided to this study by the National Science Council, Taiwan under the grant no. 100-2221-E-020-012.

References

[1] K.H. Tseng, K.J. Chuang, Application of iron-based powders in tungsten inert gas welding for 17Cr–10Ni–2Mo alloys, Powder Technology 228 (2012) 36–46.
[2] K.H. Tseng, K.L. Chen, Comparisons between TiO_2- and SiO_2-flux assisted TIG welding processes, Journal of Nanoscience and Nanotechnology 12 (2012) 6359–6367.
[3] H.Y. Huang, Effects of activating flux on the welded joint characteristics in gas metal arc welding, Materials and Design 31 (2010) 2488–2495.
[4] T.S. Chern, K.H. Tseng, H.L. Tsai, Study of the characteristics of duplex stainless steel activated tungsten inert gas welds, Materials and Design 32 (2011) 255–263.
[5] K.H. Tseng, C.Y. Hsu, Performance of activated TIG process in austenitic stainless steel welds, Journal of Materials Processing Technology 211 (2011) 503–512.
[6] S.M. Gurevich, V.N. Zamkov, N.A. Kushnirenko, Improving the penetration of titanium alloys when they are welded by argon tungsten arc process, Avtomaticheskaya Svarka 9 (1965) 1–4.
[7] J.J. Lowke, M. Tanaka, M. Ushio, Mechanisms giving increased weld depth due to a flux, Journal of Physics D: Applied Physics 38 (2005) 3438–3445.
[8] P.J. Modenesi, E.R. Apolinário, I.M. Pereira, TIG welding with single-component fluxes, Journal of Materials Processing Technology 99 (2000) 260–265.
[9] R. Sudhakaran, V. VeL Murugan, K.M. Senthil Kumar, R. Jayaram, A. Pushparaj, C. Praveen, N. Venkat Prabhu, Effect of welding process parameters on weld bead geometry and optimization of process parameters to maximize depth to width ratio for stainless steel gas tungsten arc welded plates using genetic algorithm, European Journal of Scientific Research 62 (1) (2011) 76–94.
[10] N.B. Mostafa, M.N. Khajavi, Optimisation of welding parameters for weld penetration in FCAW, Journal of Achievements in Materials and Manufacturing Engineering 16 (2006) 132–138.
[11] P.C. Tseng, K.H. Tseng, Activating flux for welding stainless steels, United States Patent US 7,896,979 B2 (2011) 1–11.
[12] M.L. Lin, T.W. Eagar, Influence of arc pressure on weld pool geometry, Welding Journal 64 (6) (1985) 163–169.
[13] M.L. Lin, T.W. Eagar, Pressures produced by gas tungsten arcs, Metallurgical Transactions B 17B (1986) 601–607.
[14] S.H. Ko, S.K. Choi, C.D. Yoo, Effects of surface depression on pool convection and geometry in stationary GTAW, Welding Journal 80 (2) (2001) 39–45.